

The mechanism of laser cutting

I. Miyamoto and H. Maruo

1. Introduction

Recently laser cutting has been finding a wide variety of applications in industry due to its excellent cut quality with high productivity and flexibility. However, the mechanism of laser cutting has not been well understood, although several papers have been published [1-5] analysing laser cutting. The understanding of the mechanism of laser cutting requires systematic analysis including the physical and metallurgical properties of molten material and beam-material interaction during laser cutting.

The authors have carried out work including the characterization of cut face and cutting front, analysis of energy contributing to cutting, behaviour of molten dross, and the interaction between laser and material in laser cutting, and discussed the difference between laser cutting and conventional gas cutting. In this report, these analyses are summarized, and the mechanism of laser cutting is developed.

2. Classification of laser cutting

Laser cutting is classified into three modes as follows:

- (a) vaporization,
- (b) melting and
- (c) photochemical ablation.

Most organic materials and ceramics are cut mainly by vaporization, decomposition or photochemical ablation depending on the wavelength of the laser beam used. On the other hand, metals can be removed in a liquid state, since they have wide temperature ranges of liquid state and high fluidity of the melt. However, vaporization can also become dominant when a pulsed laser beam with high peak power is used even in metal cutting.

When oxygen gas is used for cutting metals, cutting speed is generally increased. As described later, the roles of oxygen gas in laser cutting are summarized as follows:

- (1) utilization of exothermic energy

- (2) reduction of viscosity and surface tension

- (3) increase of laser beam absorptance.

3. Properties of dross

3.1. Maximum cutting speed of various metals

(a) *Comparison between O₂ and Ar gas:* In Fig. 1, maximum cutting speed V_m is compared between Ar and O₂ gases at 1 KW of a CW CO₂ laser; V_m is the maximum speed to separate physically the plate without taking into consideration cut quality. Oxidation (exothermic) energy and melting temperatures of metal/oxide are also plotted in this figure.

In Ar cutting, the smaller the thermal conductivity and melting temperature, the faster the cutting speed, indicating

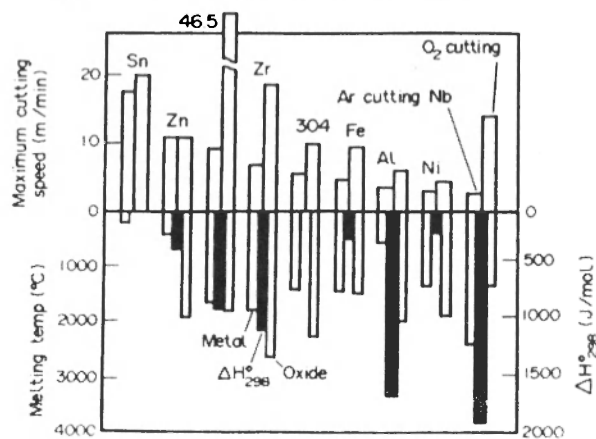


Fig. 1 : Comparison of maximum cutting speed with O₂ and Ar gases (1 kW CW CO₂ laser, 1 mm thickness)

that V_m is basically dependent on the thermal properties of the metal.

In O₂ cutting, V_m is seen to increase with increasing oxidation (exothermic) energy of the metal. The oxidation energy is relatively high in Nb, Al, Zr and Ti, and rather low in Fe and Ni. V_m is seen to be much faster in O₂ cutting than Ar cutting in Ti, Zr and Nb, showing that oxidation energy plays an important role in these metals. It should be emphasized, however, that the quality of cut surface is very much inferior in Ti, Zr and Nd. This is because the oxidation region cannot be limited to the beam irradiating region due to their large exothermic energy.

¹ I. Miyamoto and H. Maruo are at the Department of Welding and Production Engineering, Osaka University, Japan.

In Al and Zn, however, V_m in O_2 cutting is not so fast as Ar cutting. This is because the melting temperatures of the oxide formed are much higher than those of the base metal.

V_m in O_2 cutting in steels is also not as fast as Ar cutting in thin metal, due to comparatively small oxidation energy. However, O_2 cutting of Fe (mild steel) provides the best cut quality in metals tested, because the reaction zone is limited to the beam irradiated region due to its low exothermic energy.

(b) *Impurity in O_2 gas:* The effects of an N_2 impurity were also examined on V_m in mild steel. As seen in Fig. 2, V_m decreases quickly as N_2 content increases at N_2 contents less than 100%. This suggests that higher

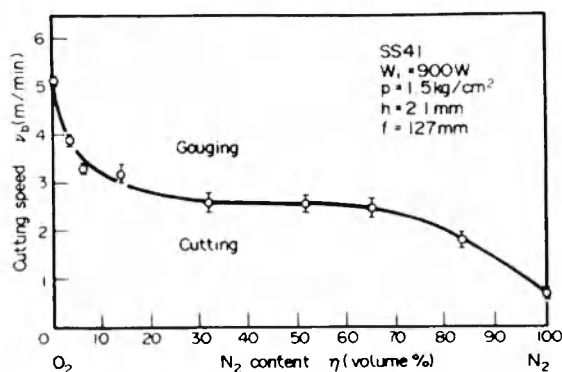


Fig. 2 : N_2 content vs. maximum cutting speed in cutting mild steel (2.1 mm)

cutting speeds can be attained by using O_2 gas with purities higher than commercially available. In a region between 15 and 70% N_2 , V_m is almost constant, nearly half of pure O_2 cutting. The cut surface, on the other hand, becomes smoother especially near the top surface, as N_2 content increases, as seen in Fig. 3. It is also seen that the cut quality near the bottom surface is reduced as the N_2 content increases, which is due to increase in viscosity of the melt as will be described later.

3.2. Viscosity and surface tension of dross

Cut quality and attainable cutting speed strongly depend on how smoothly the dross can be removed from the cutting zone. The dross removal is affected by viscosity and surface tension of the dross.

(a) *Surface tension:* High surface tension can prevent the dross flowing smoothly out of the reaction zone. The surface tension of metal is normally higher than that of its oxide as shown in Table 1; the surface tension of Fe

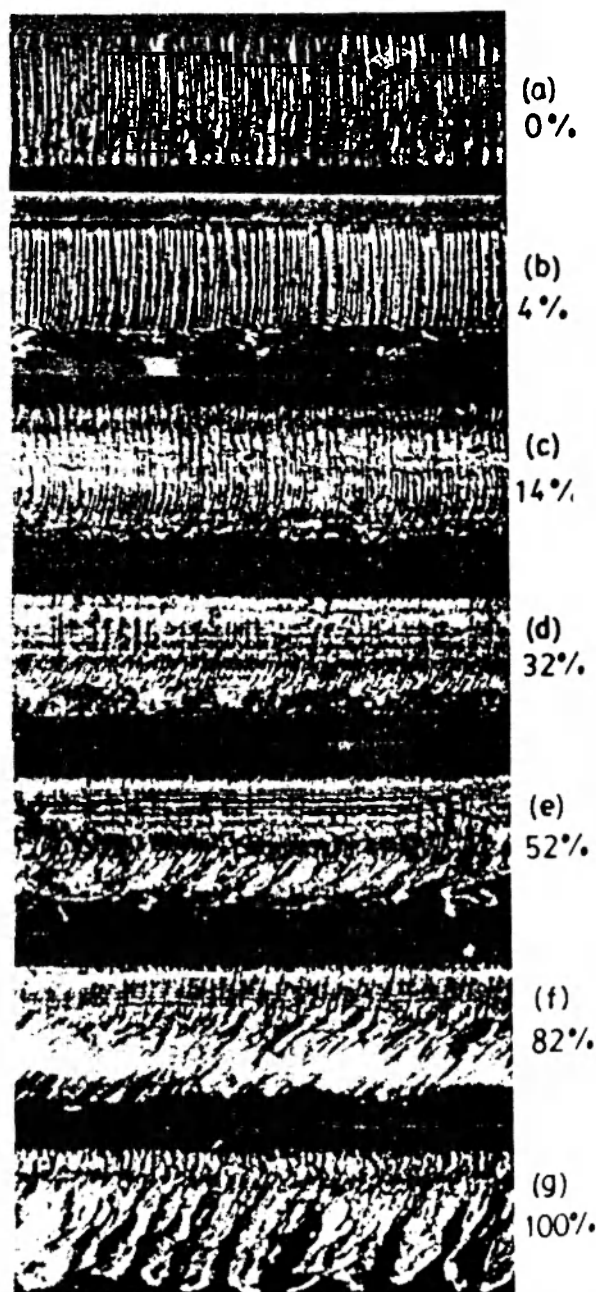


Fig. 3 : Cut surface appearance corresponding to Fig. 2

	Temperature (°C)	Surface tension (dyne/cm)
Fe	1570	1700—1800
Cu	1083	1350
Al_2O_3	2050—2400	360—570
Cr_2O_3	2350—2500	810
FeO		580

is approximately three times higher than that of FeO. Thus in Ar-laser cutting dross free cutting is accomplished only at high pressures in comparison with O₂ cutting.

(b) *Viscosity*: Figure 4 shows the viscosity of Fe and FeO plotted against temperature; although the viscosity of FeO is higher than that of Fe at low temperatures, it decreases quickly with increasing temperature, becoming lower than that of Fe at >1700°C. As is described later, temperature at the cutting front, ranging from 1800 to 2500°C in CW O₂-laser cutting, is much higher than that of conventional gas cutting (1600-1700°C). Lower viscosity is required in faster cutting, because a higher rate of dross removal is required. Narrower kerf also requires higher temperatures, since it has a larger resistance to dross flow. Thus it is now reasonable to assume that a high cutting speed and narrow kerf with smooth surface can be attained at high temperatures.

(c) *Pile cutting of stainless steel*: Type 304 stainless steel is known to have a strong tendency to dross attachment,

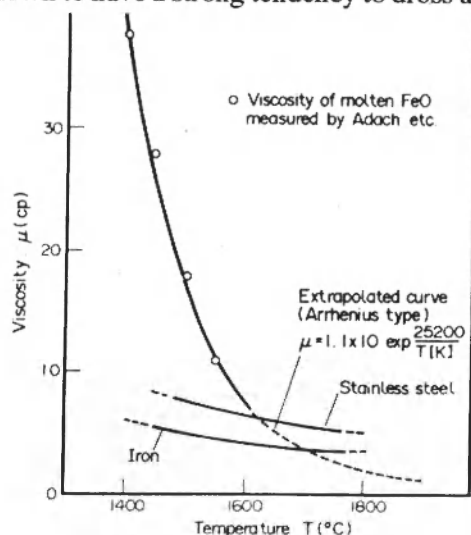


Fig. 4. : Relationship between viscosity and temperature of steels and FeO

so that the cut quality is normally not as good as mild steel. This is because chromium oxide has a high viscosity and high surface tension. The cut quality of 304 stainless steel can be very much improved by reducing the viscosity and surface tension of the dross; reduction of dross viscosity and surface tension can be realized by “pile-cutting” [7] where a thin mild steel plate is placed on 304 steel, as shown in Fig. 5. As seen in the FeO-Cr₂O₃ phase diagram in Fig. 6, FeO from mild steel dilutes the Cr₂O₃ concentration so that the viscosity and surface tension of the dross are reduced. Thus pile cutting provides completely dross-free cutting along with a smooth cut face, as shown in Fig. 7. A similar improvement was also observed in cutting Ni plates, in

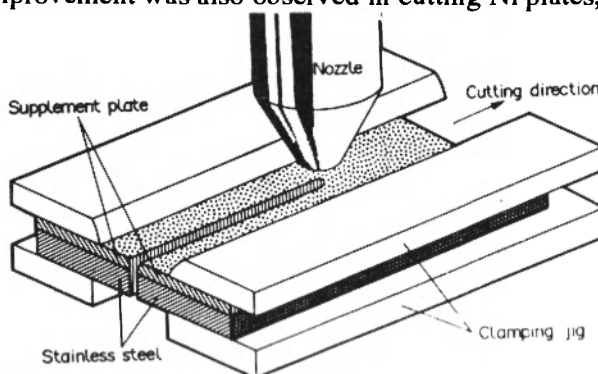


Fig. 5 : Arrangement of pile cutting of stainless steel

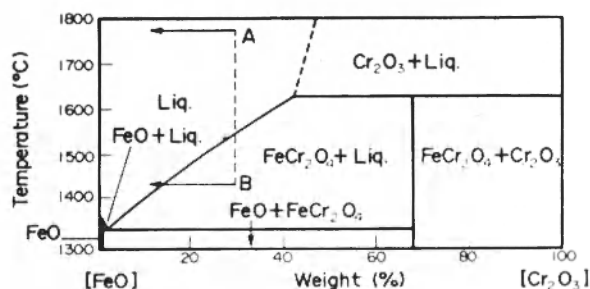


Fig. 6 : Phase diagram of FeO-Cr₂O₃ system

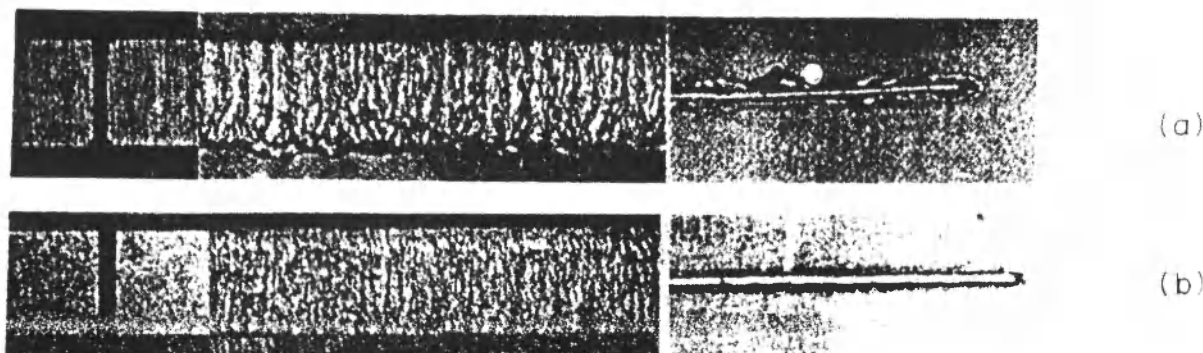


Fig. 7. : Comparison of cut face of 304 steel between normal cutting (a) and pile-cutting (b) (3 m/min)

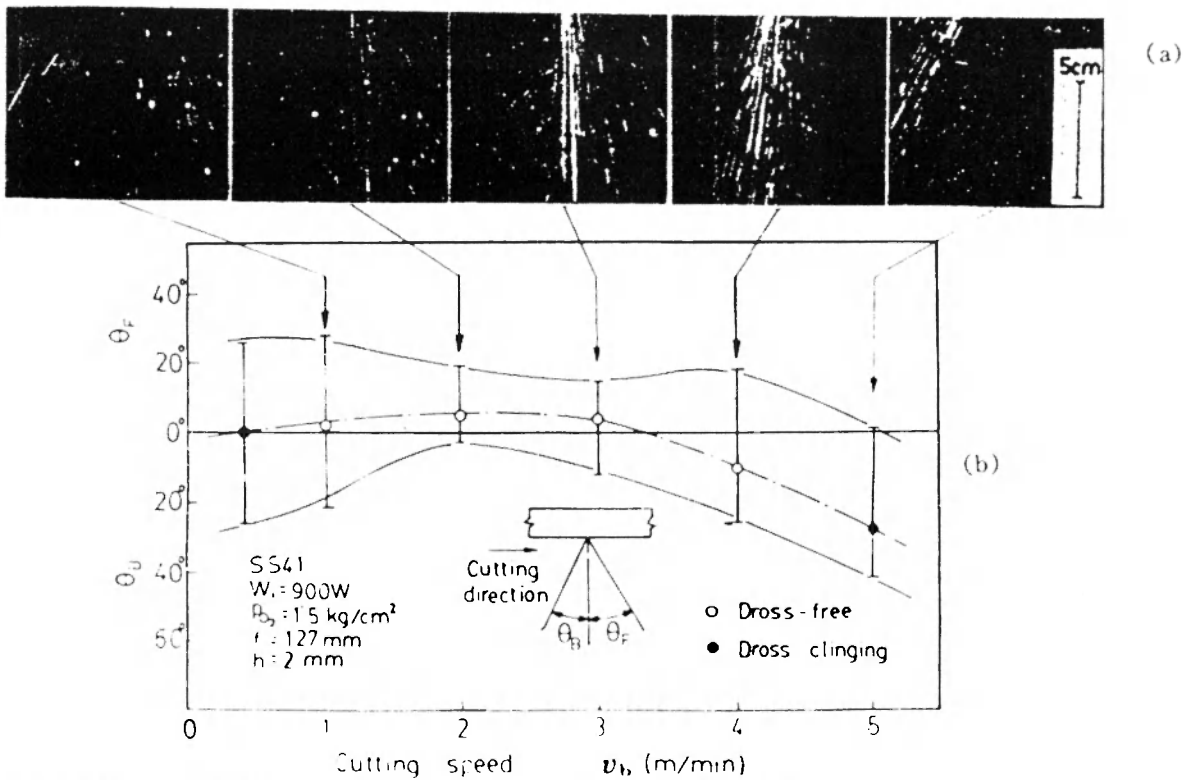


Fig. 8 : Mean angle of dross shower vs cutting speed (see Figs 9-11)

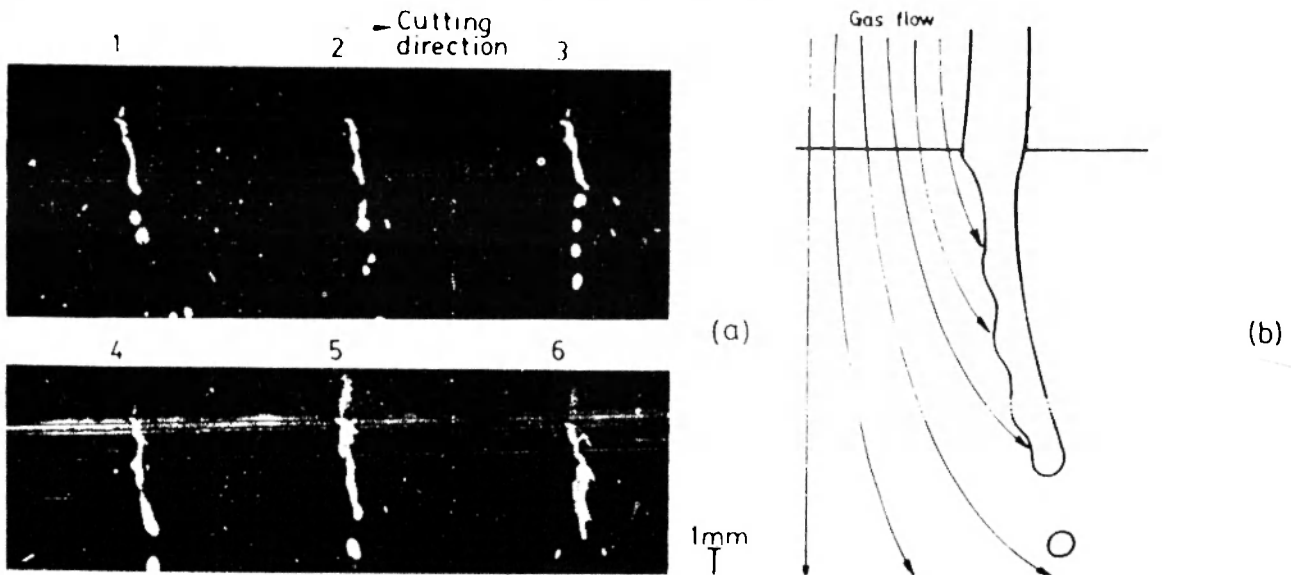


Fig. 9 : High speed movie pictures of dross flow (dross free, frame to frame : 3.3 ms)

which dross tends to attach to the rear surface in normal laser cutting.

Another possibility of reducing viscosity and surface tension is by elevating the dross temperature. This can be realized by using a well focused laser beam or a pulsed laser beam as will be described later.

3.3 Behaviour of dross attachment

(a) Angle of dross shower: Pictures of the dross shower were taken from the side with a 35 mm camera. The

mean angle of the dross shower is inclined a little forward in dross-free cutting as shown in Fig. 8. The direction tends to become backwards at higher and lower speeds where dross attachment was observed.

(b) High speed filming: High speed films were taken to observe dross flowing out of the rear surface. In dross-free cutting at 2m/min, a string-like dross is seen to flow away along the cutting front, and the oxygen gas flow appears to push the string of the dross forward (Fig. 9). At higher cutting speeds, the dross stream

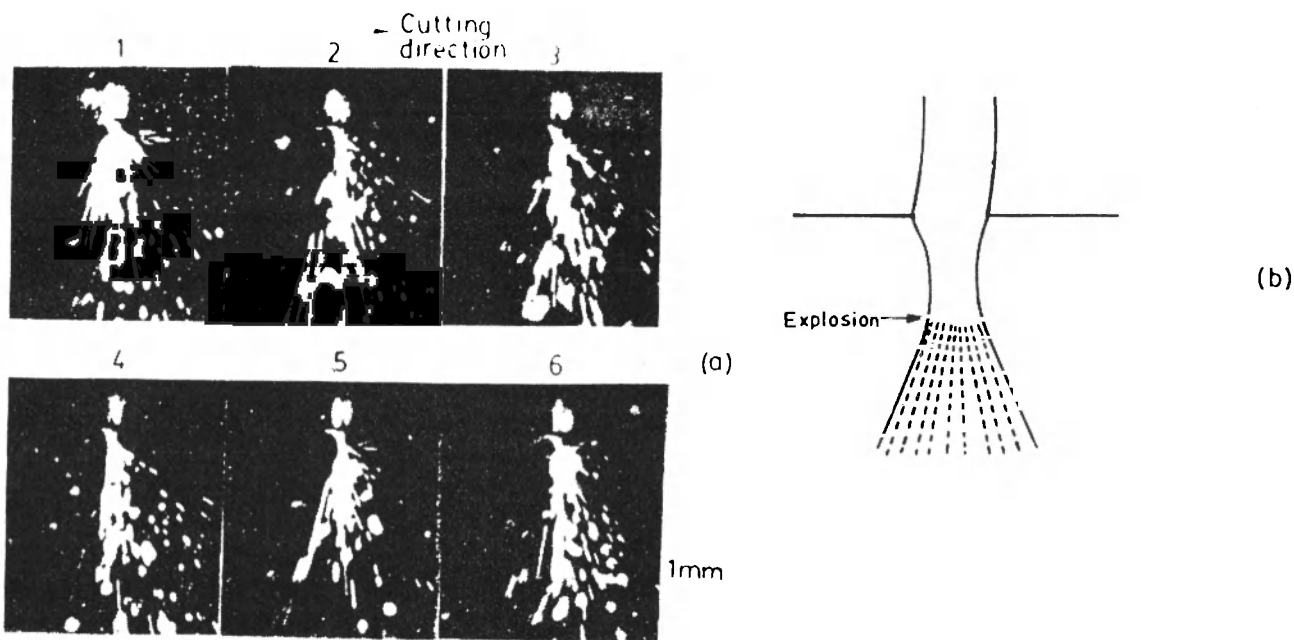


Fig. 10 : High speed movie pictures of dross flow (dross free, frame to frame : 2.8 ms)

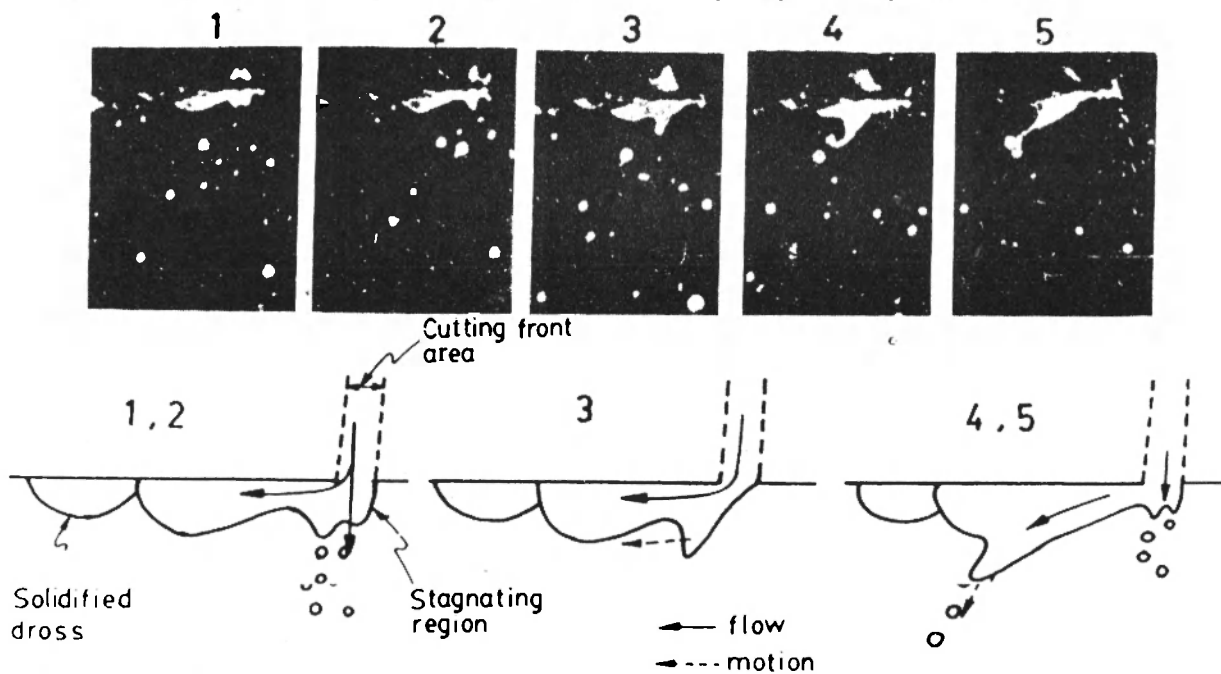


Fig. 11 : High speed movie pictures of dross flow (dross attachment, frame to frame : 2.2 ms)

becomes spray-like flow, which tends to incline backwards (Fig. 10). Dross attachment begins when the inclination angle becomes larger.

Figure 11 shows dross attaching at lower speed, 0.8 m/min; the dross flow is seen to be pulled back by the molten pool behind the cutting region, and thus the shower tends to incline backwards. The dross was observed to be more clearly pulled back by the molten dross in stainless steel.

3.4 Absorptance at the cutting front

(a) *Reflection at the cutting front:* The laser beam intensity pattern passed through thin steel plate was recorded by using an acrylic sheet placed underneath. Figure 12 shows the bum patterns and the shape of cutting front, which was obtained by inserting a Cu plate quickly between workpiece and nozzle. The beam pattern thus obtained is seen to locate behind the beam axis showing that the laser beam is reflected at the cutting front. The amount of

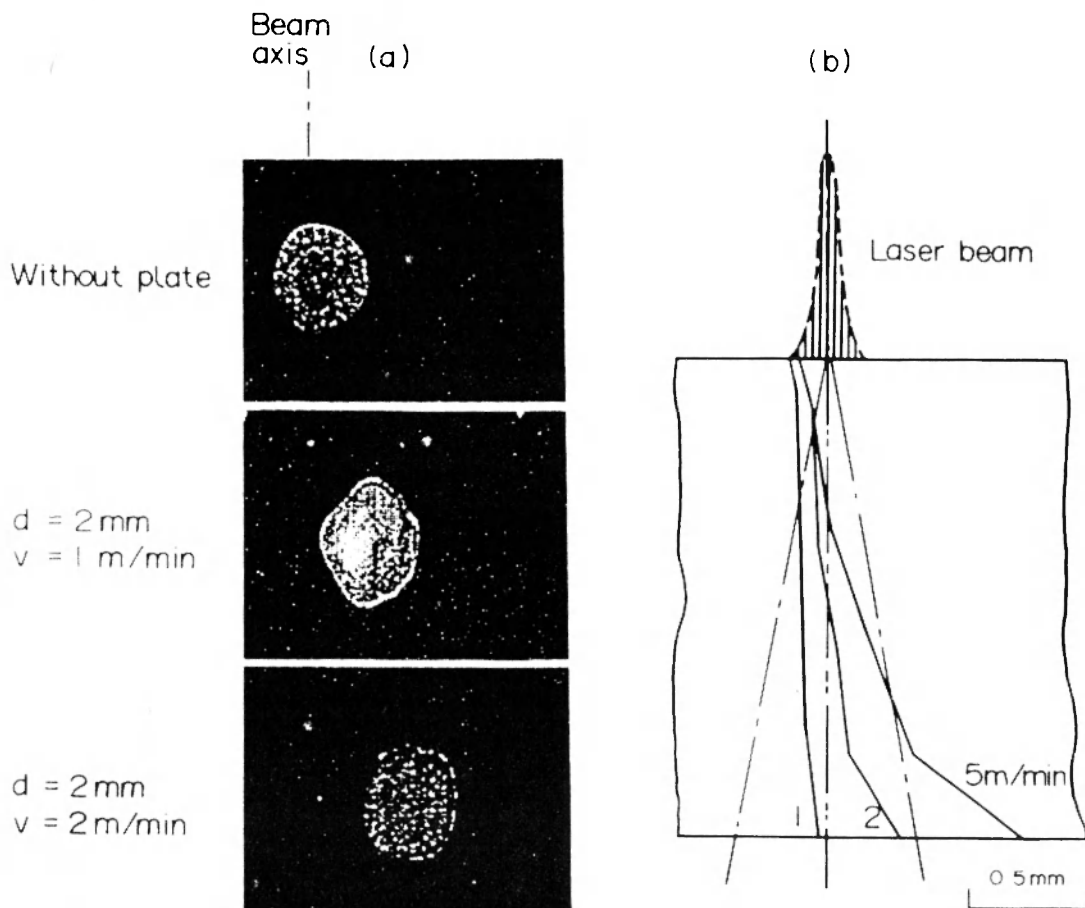


Fig. 12 : Beam pattern passed through the plate (a) and shape of cutting front (b)

displacement increases as the cutting speed increases, because the tilting angle of the cutting front increases.

(b) **Absorptance at room temperature:** Since the cutting front is covered with molten oxide in O₂-laser cutting, CO₂ laser absorptance is expected to be much higher than that of metal. Absorption characteristics of random or circular polarized CO₂ laser beams is discussed here, since the effect of linear polarized laser beams is well covered by Olsen [8].

First, absorptance of polished mild steel plate was estimated at room temperature by measuring the reflected CO₂ laser power with random polarization. The specimen was prepared by heating at 500°C in the air. Figure 13 shows the relationship between incident angle and absorptance at low laser power. The absorptance increases with increasing heating time, and almost saturates in 10-15 min to approximately 60% at normal incidence. The maximum absorptance was 35-40% near 85°, which approximately corresponds to the incident angle at the cutting front.

The absorptance of the cutting front was also estimated by measuring the reflected laser power during laser cutting, which passes through the plate. An experiment

was performed at a cutting speed to provide the geometry of cutting front where all incident laser beam is single-reflected. The absorptance thus estimated was found to be in a range of 60-70%, which is considerably larger than the aforementioned value, 35-40%, estimated at room temperature (see Fig. 13).

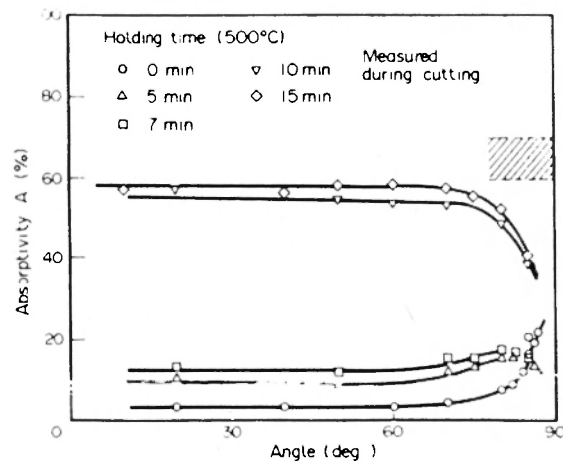


Fig. 13 : Reflectance vs incident angle of oxidized steel at 500°C for various times (random polarized CO₂ laser beam)

4. Interaction between laser beam and material

4.1. Temperature of cutting front

(a) *Temperature measurement*: It is important to estimate the temperature at the cutting front, since oxidation rate and fluidity strongly depend on the temperature. The temperature was measured by using a radiation pyrometer. Since the minimum measurable diameter of the radiation pyrometer used, approximately 0.5 mm, is larger than the kerf width (<0.3mm), the output signal was calibrated by detecting the signal from a test piece heated in an induction furnace to known temperatures through a slit with the same width as the kerf.

(b) *Effect of cutting speed*: Figure 14 shows the temperature plotted against the cutting speed; the temperature was measured at 0.4 mm from the top surface. The distance between cutting front and beam axis r_F was also measured by using a microscope.

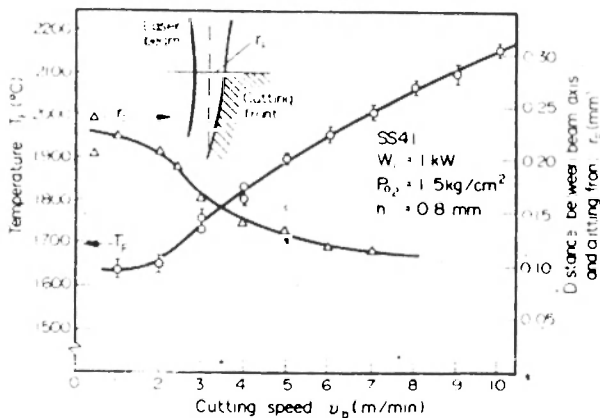


Fig. 14 : Temperature and r_F VS cutting speed at 0.4 mm from top surface (mild steel : 0.8 mm)

The temperature was found to be constant, approximately 1650°C, at cutting speeds slower than 2m/min, which is nearly the same as that of conventional gas cutting [9, 10]. At speeds faster than 2m/min, the temperature increases almost linearly with increasing cutting speed, reaching 2150°C at 10m/min. A higher temperature is seen to correspond to a smaller r_F where the intensity of the laser beam is higher. The temperature attained in CW laser cutting is not so high for plasma to be produced at the reaction zone.

In conventional gas cutting, the temperature is in the range 1600-1700°C, and the maximum cutting speed is limited to about 1.5 m/min, which is considered to be

the oxidation rate at this temperature range. Laser cutting within this speed limit is considered to be oxidation-dominant as in the case of the gas cutting. Higher cutting speeds require additional heating by laser beam. The temperature is reached by self-adjustment of r_F to provide an oxidation rate required at the given cutting speed. The temperature in stainless steel showed a similar tendency to mild steel, although the stainless steel provided temperatures 5-10% lower than mild steel [7].

(c) *Temperature distribution* : The temperature distribution was also measured along the cutting front. The temperature increased monotonically with increasing distance from the top surface at 2.5 m/min or lower as shown in Fig. 15. This tendency is reasonable,

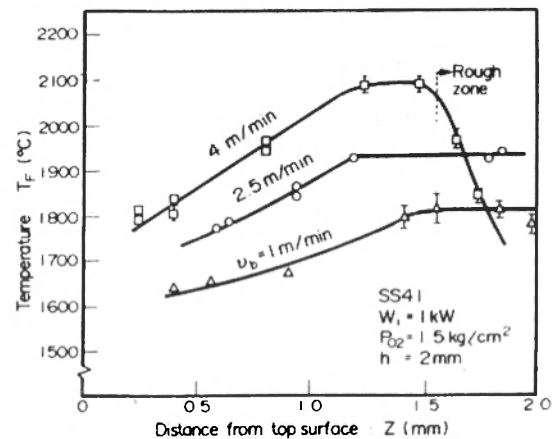


Fig. 15: Temperature distribution along thickness of cutting front of mild steel

since a higher rate of dross removal is required at the lower part of the plate.

At 4 m/min. the temperature is seen to decrease near the rear surface, and then dross was seen to attach to the rear surface, since its fluidity is not high enough due to the low temperature there, A similar tendency was observed in cutting stainless.

4.2 Thermal analysis

(a) *Laser beam energy q_L* : Laser power passed through work was measured by using a calorimeter located underneath, and the laser beam energy required to remove unit volume of material q_L was estimated by

$$(q_L)_x = (Q_x - Q_{x+h}) / v d_x h \quad \dots \quad (1)$$

where Q_x and Q_{x+h} is the laser power passed through the plate of thickness x and $x+h$, respectively, v cutting

speed and d_x kerf width. Figure 16 shows the distribution of q_L along thickness; q_L is constant, approximately 20 kJ/cm^3 , which was found to be independent of laser power, beam spot size and thickness, in dross-free cutting.

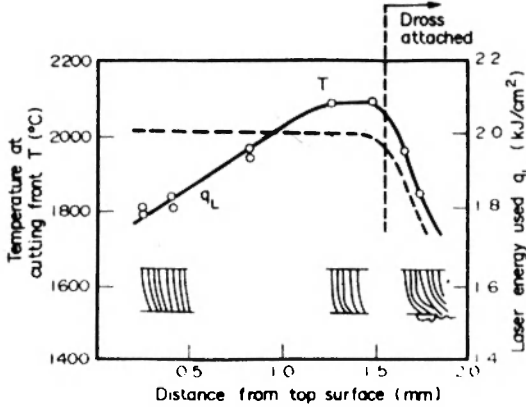


Fig. 16. q_L distribution along thickness

(b) Exothermic energy q_R : Exothermic energy q_R also plays an important role in O_2 cutting. The total energy $q_L + q_R$ is approximated by a simple model line heat source [11];

$$q_L + q_R = 8KT(vd/4k + 0.2) + KvdH/k \quad \dots \quad (2)$$

where T is the temperature at the cutting front, K thermal conductivity, k thermal diffusivity and H latent heat of fusion. q_R can be determined from Eqs (1) and (2).

In Fig. 17. q_L and q_R and plotted against cutting speed in dross-free cutting. At low cutting speeds, q_R is larger than q_L , showing speed increases, q_R decreases monotonically, becoming smaller than q_L at speeds faster than 2 m/min.

(c) Chemical composition of dross: Dross was collected in a container filled with water, and its chemical composition was analysed by X-ray diffractometry. Since the dross can be oxidized in a space between the work piece

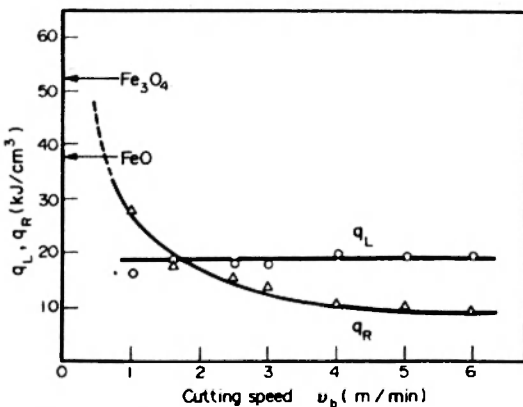


Fig. 17: q_L and q_R vs cutting speed in O_2 laser cutting mild steel

and the container, the dross was collected at various distances L_C between the workpiece and the water surface. Figure 18 indicates the relationship between chemical

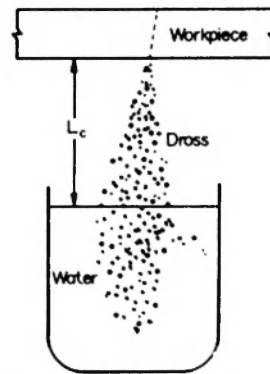
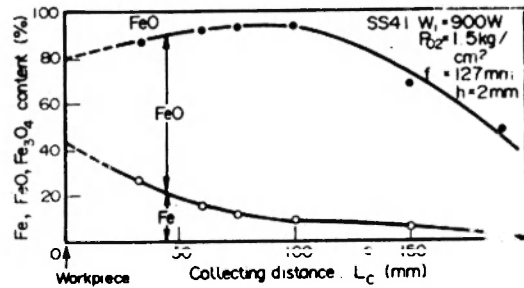


Fig. 18: Chemical compositions of dross in container at various distances L_C

composition and L_C . Fe concentration is seen to increase with decreasing L_C . The compositions at $L_C = 0$ were estimated by extrapolation of the curve at each cutting speed. The chemical composition thus estimated is shown in Fig. 19.

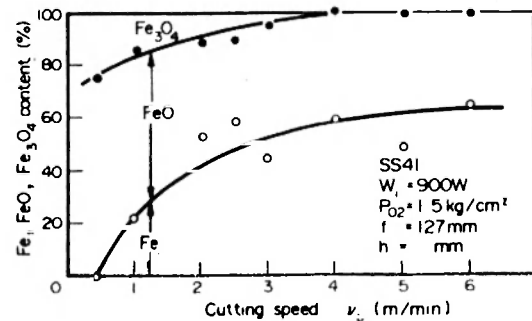


Fig. 19: Chemical compositions of dross at $L_C = 0$ plotted against cutting speeds

At low cutting speed, most iron is oxidized to form FeO or Fe_3O_4 , producing a large amount of exothermic energy; then cutting is seen to be oxidation-predominant as in the case of the gas cutting. At speeds >2 m/min, less Fe is oxidized, reducing the value of q_R (Fig. 17), as cutting speed increases.

(d) q_L during dross attachment : As shown in Fig. 16, q_L is seen to become smaller than 20 kJ/cm^3 near the bottom surface in O_2 -laser cutting with dross attachment. Correspondingly the temperature also tends to decrease (see Fig. 15), showing that the bottom part is not heated by enough laser beam energy.

4.3. Process of striation formation

(a) Causes of surface roughness : In laser cutting the cut surface is roughened by :

- (a) carriage vibration,
- (b) fluctuation of laser power, and
- (c) natural striations.

The first two items are easy to understand, and their effects on surface roughness have been quantitatively studied along with a possibility of in-process monitoring [12]. It should be noticed that the cut surface is roughened by natural striations, even without carriage vibration and laser power fluctuation.

The striations are regularly spaced, and are normally seen on the cut surface of mild steel [2]. The pitch of the striations is almost independent of cutting speed except at very low cutting speeds where cutting tends to become self-burning, and increases with increasing beam spot size.

(b) High speed filming : The formation process of natural striations was observed by high speed filming [13]. In order to obtain a general view of reaction zone, filming was first undertaken in edge-cutting where a half of the focused laser beam heats the work, as schematically

drawn in Fig. 20 (b). As seen in Fig. 21, the reaction zone is confined to the front face, and the oxidation reaction is periodically changing.

Filming of normal cutting was also undertaken from the back to see a detailed behaviour of the reaction zone as shown in Fig. 20(a). A series of pictures at low cutting speed, 1 m/min, are shown in Fig. 22. The reaction is seen to be unsteady but again changing periodically; the reaction initiates at a small point at top surface, expands to form a triangular reaction zone and slips downwards. Then a period of no reaction around the top surface follows, which continues until another bright spot initiates at the top surface again. In the lower part, a bright-reaction zone was always seen to exist but with some fluctuation. At speeds $>2\text{-}3 \text{ m/min}$, the reaction was seen to be almost continuous as shown in Fig. 23.

(c) mechanism of striation formation : Figure 24 shows the movement of various locations in the reaction zone measured by using a film analyser for cutting speeds of 0.8 and 1.4 m/min [13]. the advancing speed of the front face was calculated from this figure; the advancing speed reaches its maximum just after the beam spot touches the front face. This speed can become greater than the cutting speed at the moment the exothermic energy emerges by the ignition of oxidation due to laser beam heating. The oxidation reaction is ignited by the laser beam. The maximum speed V_r is plotted against cutting speed in Fig. 25. The front face moves at the same speed as the cutting speed at cutting speeds faster than 2 m/min. Speeds of other cutting zones are also plotted in Fig. 25.

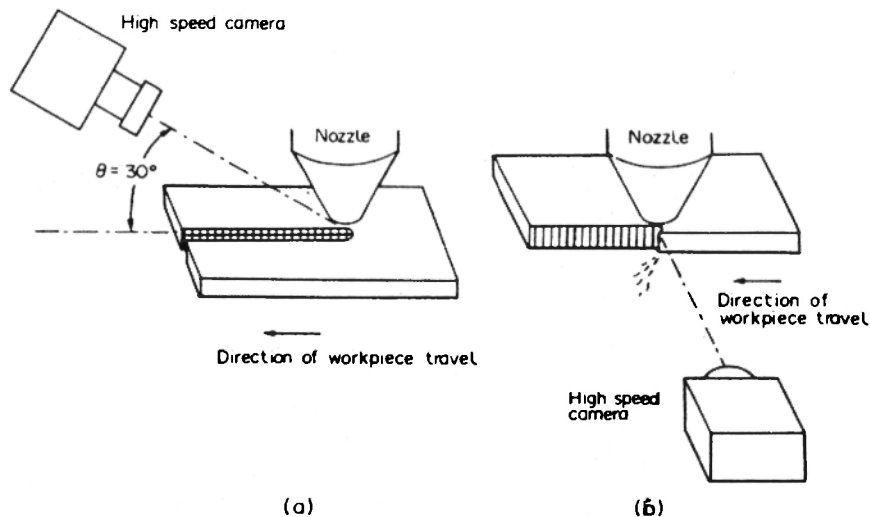


Fig. 20 : Schematic illustration showing laser cutting

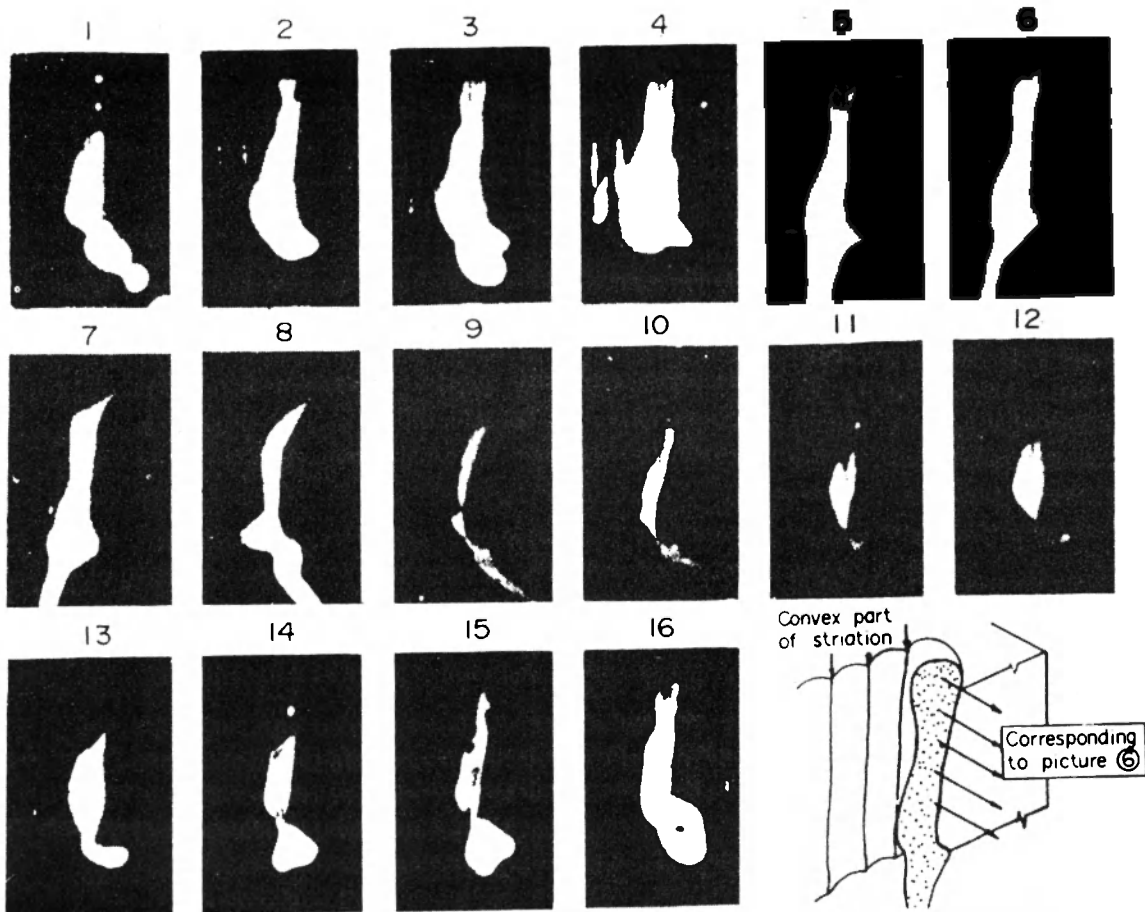


Fig. 21 : High speed movie pictures in laser edge cutting of mild steel (1.2 mm, 80 cm/min, frame to frame : 1 ms)

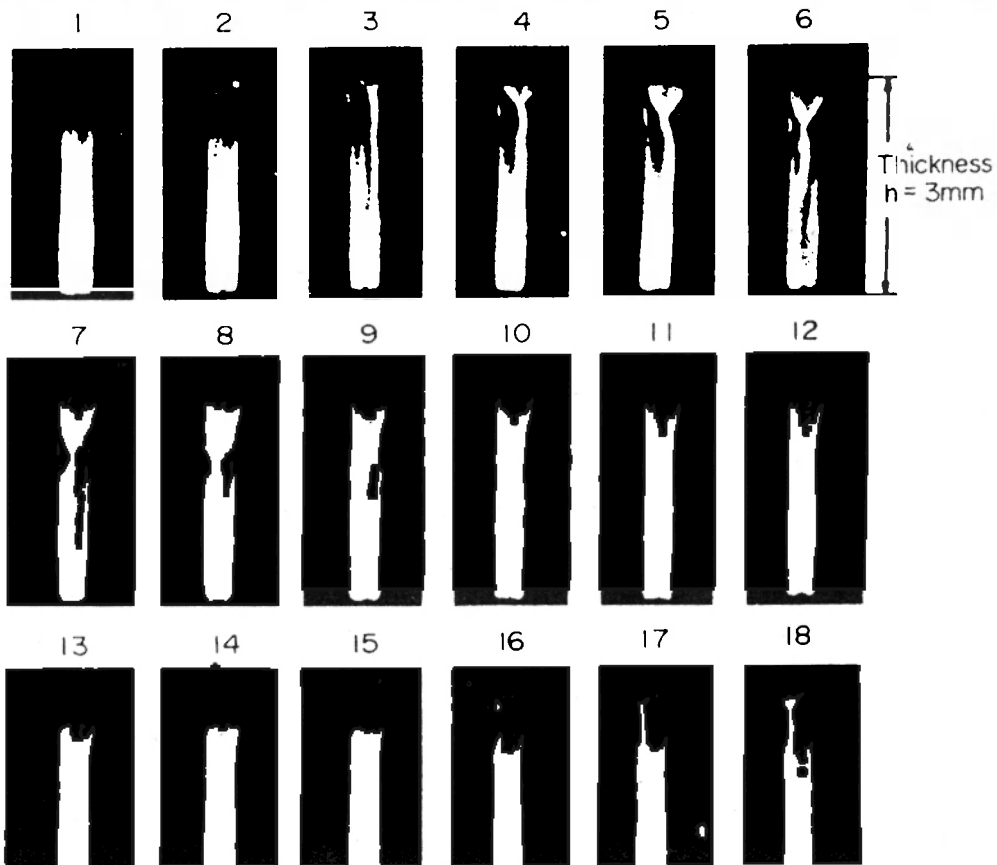


Fig. 22 : High speed movie pictures in normal laser cutting of mild steel (3 mm, 1 m/min, frame to frame : 1 ms)

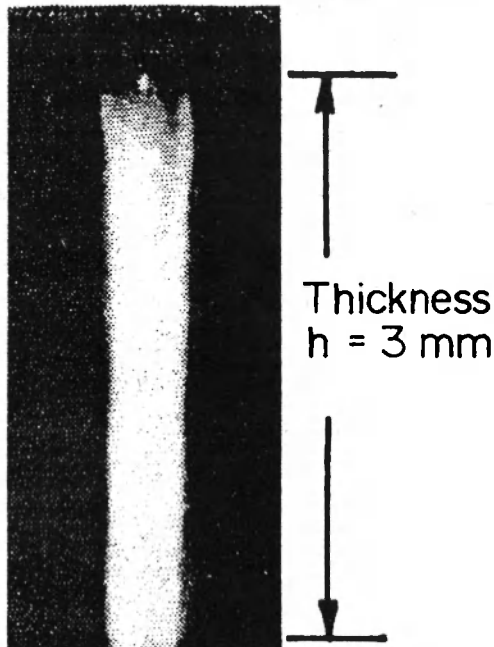


Fig. 23 : Laser cutting at 2.5 m/min. Little fluctuation was observed

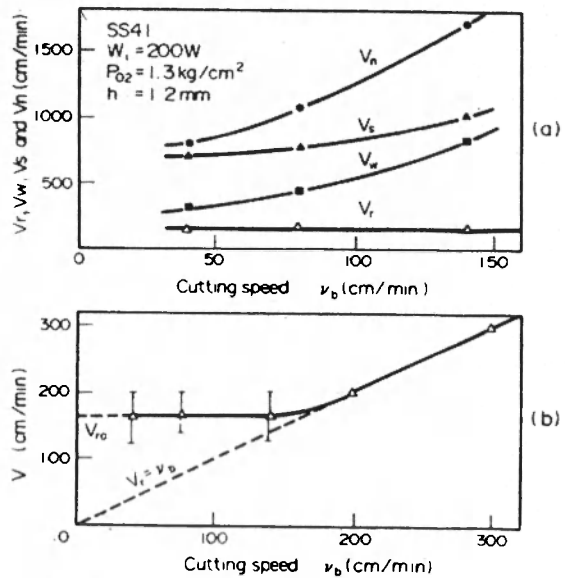


Fig. 25 : Moving speed of reaction zone in laser cutting

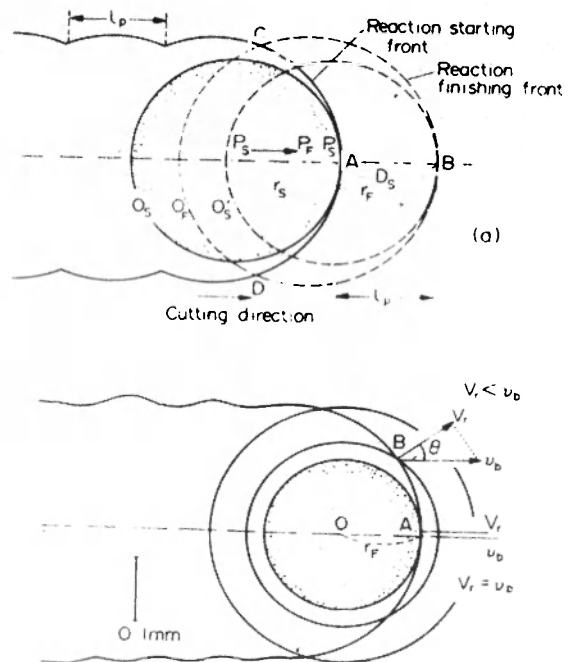


Fig. 26 : Interaction between laser beam and cutting front. (a) Striation formation at low speed; (b) continuous cutting at high speed

the oxidation rate, about 1.5 m/min, is faster than cutting speed. The cutting front can proceed within the heat affected zone where the oxidation reaction can be maintained due to laser heating. Then no reaction occurs until the laser beam catches up with the cutting front again. One cycle of the reaction was confirmed to be the same as a space of the striation. At cutting speeds faster than the oxidation rate, the front face cannot move ahead of the laser beam, so that the front face and the laser beam move at the same speed as shown in Fig. 26 (b).

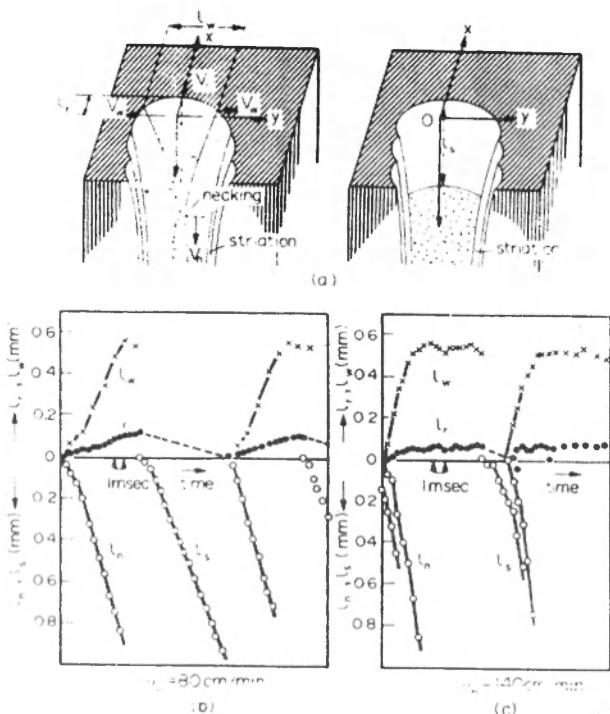


Fig. 24 : Periodical movement in reaction zone observed in high speed movie pictures

Figure 26 (a) illustrates the mechanism of striation formation developed on the basis of this analysis. At cutting speeds $< 1.5\text{-}2 \text{ m/min}$, oxidation is ignited by a high power laser beam when it touches the cutting front. Then the cutting front moves ahead of the laser beam, because

In this simplified model, since oxidation speed is assumed to be constant, 1.5-2 m/min, which corresponds to the value of 1600-1700°C, no periodic reaction should occur at speeds faster than 1.5-2 m/min.

In actual O₂-laser cutting, however, reaction rates faster than 1.5-2 m/min are attained, because the front face is heated to higher temperatures by laser heating. Thus the oxidation rate can become faster than the cutting speed due to release of exothermic energy only. Fine striations are still seen even at speeds >3 m/min. However, the cutting front can move ahead of the laser beam by very small distance. This was not visible in high speed films, due to very high temperature gradient. A very smooth cut face, $R_z = 0.8$ [14] can be attained by using a very stable CO₂ laser.

4.4 Pulse laser cutting

The temperature at the cutting front was measured in O₂ cutting using a pulsed CO₂ laser. Figure-27 shown an example of the results. The temperature is much higher than CW laser cutting, at the top surface it reaches

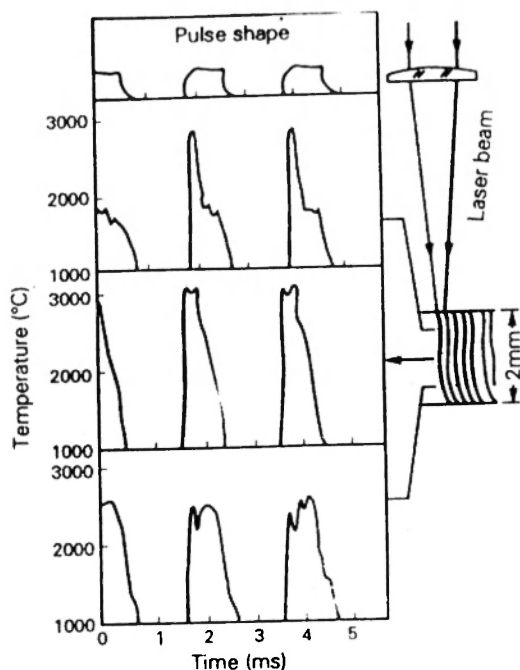


Fig. 27 : Temperature at the cutting front in PW laser cutting of 2 mm mild steel

almost 3000°C at the leading edge of the pulse. Such a high temperature is attained by intense beam irradiation at a high peak power with small r_F at normal incidence

because the cutting front approaches the beam axis during the off period of the pulse.

It should be also noticed that temperature decreases to a value lower than 1000°C, at which oxidation reaction cannot be maintained. Since the reaction zone is very quickly heated to a high temperature, material can be removed with negligible thermal conduction. Since it is cooled down to a low temperature during the off cycle, the heat affected zone becomes much smaller than with CW laser cutting.

Temperatures as high as 3000°C, however, cause evaporation at the cutting front, so that cutting speed is drastically reduced to a value much lower than that of CW cutting, due to the large latent heat required for evaporation. However, higher peak power leads to ablation cutting with excellent quality in materials which are difficult to be cut by CW lasers; excellent cuts of Al [15] and stainless steel [16] have been obtained by Q-switch CO₂ and high peak YAG lasers, respectively. This suggests the necessity of developing pulsed lasers with high peak power for quality cutting.

The cutting front is seen to be held at a high temperature somewhat longer in the middle and lower parts than top surface. At high pulse frequencies, therefore, the temperature will not decrease to a low temperature before next pulse starts, the cutting of PW laser approaches that of CW laser cutting. As seen in Fig. 28,

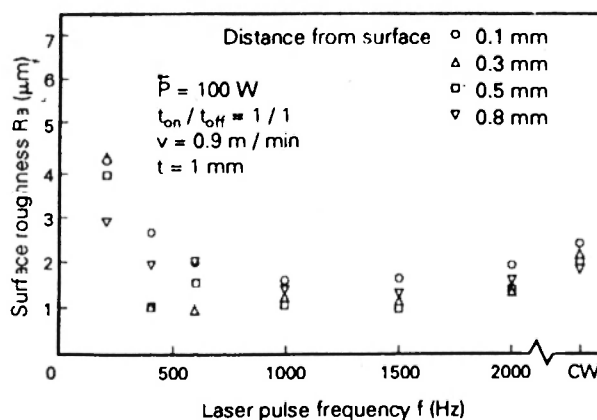


Fig. 28 : Surface roughness of PW laser cutting at various frequencies

the surface roughness of PW laser cutting approaches that of CW laser cutting. A similar tendency has been also reported by Powell *et al.* [2].

4.5. Kerf width

The laser power density was determined at the kerf edge. The beam intensity distribution was estimated by moving acrylic plastic across the focused laser beam [17]. Figure 29 shows the kerf width at top surface

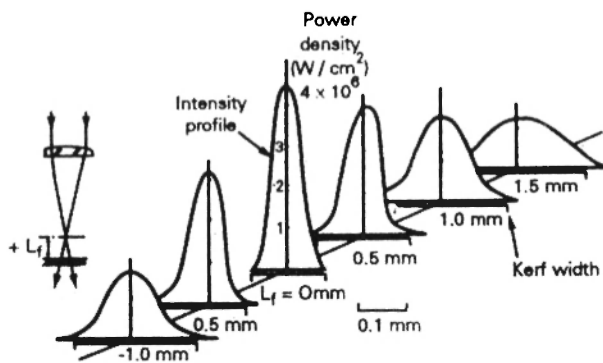


Fig. 29 : Intensity distribution of laser beam on the work and the width of top surface

obtained at various focus positions with respect to the work surface. It is seen that the kerf width is limited by the laser beam region. This is because the reaction zone shown in Fig. 26 is limited by the laser heated zone. The authors estimated the power intensity at the kerf edge more precisely by using a pyroelectric detector, and found that the power-density was around 10^5 W/cm^2 .

This suggests that clear cutting can be obtained by a laser spot with a sharp gradient at an intensity around 10^5 W/cm^2 . Since the beam portion lower than 10^5 W/cm^2 has a larger divergent angle than when diffraction limited, presumably with larger intensity fluctuation [12], a special filter of Kepler type is effective in enhancing the cut quality by removing this outer portion of the laser beam.

References

1. D. Schuocker : *The Physical Mechanics and Theory of Laser Cutting*, Industrial Laser Handbook, p. 65, 1985.
2. J. Powell, T.G. King, I.A. Menzies : Cut edge quality improvement by laser pulsing. *Proceedings of 3rd International Conference on Laser in Manufacturing*, p. 37, 1985.
3. F.O. Olsen : *The Laser Cutting Technology*, 1988 (to be published).
4. D. Petring, P. Abels, E. Bayer, G. Herziger : *Werkstoff-bearbeitung mit Laserstrahlung. Feinwerktechnik & Messtechni*, Vol. 96, p. 364, 1988.
5. S. Biermann, R. Nuss, M. Geiger : Analytical studies on laser cut surfaces. *7th International Symposium on Gas Flow and Chemical Lasers*, 1988, SPIE, USA, 1989 (SPIE No. 1031).
6. Y. Arata, I. Miyamoto, M. Kubota : Some fundamental properties of high power CW CO₂ laser beam as a heat source. *IIW Doc. IV-4-69*, 1969.
7. Y. Arata, H. Maruo, I. Miyamoto, S. Takeuchi : Improvement of cut quality in laser cutting stainless steel. *Proceedings of International Laser Processing Conference, Anaheim*, 1981.
8. F.O. Olsen : Cutting with polarized laser beam. *Lectures of the International Beam Technology Conference*, p. 197, 1980.
9. K. Teske : Contribution to explanation of gas cutting process. *Schweissen und Schneiden*, Vol. 9, No. 8, p. 122, 1956.
10. H. Hofe : New information on the mechanism of gas cutting. *Schweissen und Schneiden*, Vol. 19, No. 5, p. 213, 1967.
11. A.A. Wells : Heat flow in welding. *Welding Journal*, Vol. 31, No. 5, p. 263, 1952.
12. I. Miyamoto, T. Ohie, H. Maruo : Fundamental study on in-process monitoring in laser cutting. *4th International Colloquium on Welding and Melting by Electrons and Laser Beam*, p. 683, 1988.
13. Y. Arata, H. Maruo, I. Miyamoto, S. Takeuchi : Dynamic behavior in laser gas cutting of mild steel *Trans. JWRI*, Vol. 8-2, p. 15, 1979.
14. T. Koizumi : Features of industrial CO₂ lasers. *WG of Japan Laser Processing Committee, WG-88-0013*, 1988 (in Japanese).
15. M.V. Hoesslin *et al.* : Cutting of aluminium with a CW and repetitively pulsed CO₂ laser system. *7th International Symposium on Gas Flow and Chemical Lasers*, 1988, SPIE, USA, 1989 (SPIE No. 1031).
16. T.M.W. Weedon : private communication.
17. I. Miyamoto, H. Maruo, Y. Arata : Intensity profile measurement of focused CO₂ laser beam using PMMA. *Proc. ICALEO '84, Boston*, 1984. ■